Pd/ZEOLITE-BASED CATALYSTS FOR THE PREFERENTIAL CO OXIDATION REACTION: ION-EXCHANGE, Si/Al AND STRUCTURE EFFECT.

M. Navlani-García, I. Miguel-García, Á. Berenguer-Murcia, D. Lozano-Castelló and D. Cazorla-Amorós

Alicante Materials Institute and Inorganic Chemistry Department, University of Alicante, 03080 Alicante, Spain

ABSTRACT

A screening of Pd/zeolite-based catalysts in the PrOx-CO reaction in H_2-rich streams was performed using zeolites with different cations (H^+, Na^+ and Cs^+) prepared by ion-exchange and framework type (MFI and FAU). The assessment of the catalytic performance displayed by these zeolite-based samples revealed that both parameters play an important role in the catalytic behaviour. The optimisation of both parameters led to the preparation of an optimum catalyst, which showed high CO conversion and CO selectivity during long-stability tests.

1.   Introduction

In the last few years, energy consumption has raised to very high levels due to both worldwide population increase and technological development. The demand for energy is steadily growing and fossil fuels reserves are diminishing. Oil, coal, and natural gas supplies are not replenished as they are consumed, so an alternative energy source must

be found. In this sense, the development of a hydrogen-based economy is gaining much attention, since H_2 is an energetic vector with many advantages with respect to fossil fuels. The most important aspect is the possibility of obtaining clean energy directly from H_2 and O_2 that would produce water as the only product. To do that, one of the most viable perspectives is the implementation of hydrogen fuel cells. These are devices which would produce energy directly from the electrochemical reaction between hydrogen and oxygen. However, there are several drawbacks to overcome for the implementation of this technology. One of them is that each of the different hydrogen sources contains pollutants in different concentrations, and tolerance of the electrodes of the fuel cells is very low to many of the pollutants contained in H_2 streams. Therefore, it is mandatory to diminish the amount of the unwanted gases to levels that the fuel cells can tolerate. One of the gases which must be completely removed from the H_2 streams is CO. This gas is obtained from the steam reforming reaction in which H_2 is produced. To remove the CO generated, the first step is the water-gas shift (WGS) reaction, that usually takes place in two consecutive steps at different temperatures. However, the CO concentration exiting the WGS reactor is still too high for the entrance of the fuel cells. Therefore, an additional step is necessary to further diminish the CO concentration. Nowadays, several options are available, such as gas separation with membranes, pressure-swing adsorption, the methanation process and the Preferential CO Oxidation reaction (PrOx-CO). The objective of these processes is to diminish the CO levels below 10 ppm, which is the tolerance level of the Pt electrodes used in the fuel cells [1].

The Preferential CO Oxidation reaction (PrOx-CO) is one of the most promising and economic approaches to achieve acceptable CO concentrations in the hydrogen stream after the water–gas shift reactor, under temperatures between those of the WGS reactor and the fuel cell operation temperatures (80-200 ºC) [2, 3]. In order to perform the PrOx-CO reaction, several kinds of active phase catalysts have been studied, being the most representative those based on supported gold catalysts, supported Pt-based catalysts and other noble metal (Pd, Rh, Ru, Ir) [4]. In this regard, the low activity and selectivity of Pd-supported catalysts for PrOx-CO was confirmed by many authors [2, 5, 6]. The low activity at low temperature was explained by the formation of a hydride suppressing the possibility of CO oxidation, whereas at higher temperature metallic Pd preferentially adsorbs hydrogen rather than CO, and the adsorbed H species are more easily oxidised by the surface Pd oxide species than CO. However, a study carried out

in our research group indicated that the use of polymer-protected palladium-based nanoparticles supported on Al_2O_3 could be useful in the PrOx-CO reaction [7, 8].

Concerning the catalyst support, alumina is the most common support for noble metal-based catalysts [9-11]; however, it was found that the selectivity towards CO oxidation can be improved using a different support and several studies have pointed out that the use of zeolites as support for noble metal catalysts could be promising to improve their performance [2, 12, 13]. In addition, the zeolite matrix can facilitate the formation of active sites for different catalytic reactions, e.g. oxidation of aliphatic chlorinated volatile organic compounds [14], combustion of toluene [15], methylation of benzene by methanol [16] and so forth. In fact, zeolites constitute the most important group of heterogeneous catalysts with large scale application in refining and petrochemistry and are also widely used in environmental catalysis [17]. The ability of zeolites to be used in many fields is related to their tunable properties, which can be controlled by selecting the charge-balancing cation, the framework structure and the zeolite composition. Most of the catalytic systems in which zeolites are studied as catalysts in the PrOx-CO reaction use Pt or Au as active phase and the metal is incorporated to the zeolite structure by an ion exchange procedure [18, 19] or an impregnation method [19-21]. However, the use of different active phases or different preparation methodologies is scarcely found in the literature.

Thus, bearing these considerations in mind and the experience that our group has in the synthesis of palladium nanoparticles, the aim of the present work was to prepare catalysts based on palladium nanoparticles supported on zeolites with different ion-exchanged cations and framework type and assess the effect of these zeolite characteristics in the catalytic performance in the PrOx-CO reaction. The selected zeolites were ZSM-5 (MFI Framework type with 3-dimensional channels and pores system consisting of 10-membered-rings with opening channel diameter of 0.51x0.55 and 0.53x0.56 nm) and Y (FAU Framework type with 3-dimensional channels and a pore system consisting of 12-membered rings with opening channel diameter of 0.74x0.74 nm). Both zeolites were ion-exchanged with three different cations, H^+, Na^+ and Cs^+. Once the catalysts were prepared and characterised, their catalytic performance in the PrOx-CO reaction was evaluated.

2.   Experimental

2.1 Synthesis and purification of nanoparticles

Palladium nanoparticles were synthesized following the reduction by solvent method, as it was previously reported in a work published by our research group [7]. The palladium precursor was Pd(ac)$_2$ (98%,Sigma–Aldrich) and the capping agent used was polyvinylpirrolidone (PVP, 40 K, Sigma–Aldrich). The experiments were carried out in an inert Argon atmosphere by means of a Schlenk system.

For solution 1, 1.114 g (10 mmol) of PVP (capping agent) were added to 120 ml of ethylene glycol in a three-necked round-bottomed flask and the solution was stirred at 80 ℃ for 2 h, using a magnetic stirrer and an oil bath.

For solution 2, 0.2245 g (1 mmol) of Pd(ac)$_2$ (palladium nanoparticles precursor salt) were dissolved in 50 ml of dioxane by stirring for 2 h at room temperature using a magnetic stirrer. This solution was light orange in colour.

Solution 1 was cooled to 0 ℃ with an ice bath and 3 ml of 1M NaOH solution were added under stirring in order to adjust the pH of the resulting mixture. Then, solution 2 was poured into solution 1 under vigorous stirring to ensure homogenisation and the final mixture was heated at 100 ℃. The solution changed its colour from light orange to dark brown, which indicated that the metallic colloid had formed [22]. After that, the heating was maintained for 2 h and then the bath was removed and the colloidal suspension was cooled to room temperature.

The resulting suspension presented high stability against sintering and it could be stored under ambient conditions without formation of aggregates for periods of time over one year.

Once the colloids were prepared as described previously, the palladium nanoparticles were purified and redispersed in methanol. The purification was based on pouring an aliquot of nanoparticles colloid into a glass bottle, adding an excess of acetone and shaking the solution. As we previously reported [23], this treatment with acetone produced the extraction of the protecting polymer to the acetone phase and flocculation of the metallic nanoparticles. After discarding the supernatant organic phase, the purified nanoparticles were redispersed by gentle stirring in a known amount of methanol, so that the final suspension concentration was perfectly known.

2.2 Catalyst supports preparation

In this work, six catalyst supports were used. In order to prepare the ion-exchanged ZSM-5 and Y zeolites (in H^+, Na^+ and Cs^+ forms) a conventional ion-exchange method was used. The initial zeolites were NH_4-ZSM-5 (provided by Zeolyst International) and Na-Y (provided by Sigma-Aldrich).

In the case of ZSM-5 zeolite, H-ZSM-5 was obtained directly by conversion of the commercial form (NH_4-ZSM-5) by heat treatment in air at 450 ºC for 6 h, with a heating rate of 5 ºC/min. Na-ZSM-5 zeolite was prepared by ion exchange of the H-zeolite with $NaNO_3$ (0.2 M) as Na^+ precursor, and Cs-ZSM-5 zeolite was subsequently obtained by ion exchange of Na-ZSM-5 with $CsNO_3$ (0.1 M) as Cs^+ precursor and keeping under stirring in a thermostatic bath at 60 ºC for 1 h.

For Y zeolite, the H-Y form was obtained by ion exchange of the commercial form (Na-Y) by using NH_4NO_3 (1 M) and keeping under stirring in a thermostatic bath at 30 ºC for 24 h and subsequent heat treatment in air at 450 ºC for 6 h, with a heating rate of 5 ºC/min. The Cs-Y zeolite was directly obtained by ion exchange of Na-Y with $CsNO_3$ (0.1 M) as Cs^+ precursor and keeping under stirring in a thermostatic bath at 60 ºC for 1 h.

After each ion exchange step, the samples were filtered and washed with distilled water and then the zeolites were dried at 100 ºC and calcined at 550 ºC for 4 h (heating rate of 1 ºC/min). The obtained catalysts supports were denoted as H-ZSM-5, Na-ZSM-5, Cs-ZSM-5, H-Y, Na-Y and Cs-Y.

2.3 Catalysts preparation

The different catalysts studied in this work were prepared by impregnation of the zeolitic supports with the palladium nanoparticles colloid. For this purpose, 1.5 g of each support was mixed with the adequate amount of the purified nanoparticles colloid suspension in order to obtain a final metallic loading of 1 wt %. The mixtures were vigorously stirred for two days using a magnetic stirrer, to guarantee similar metal loading and dispersion in all the catalysts and then the samples were heat treated at 60 ºC to eliminate the solvent (methanol). Finally, the catalysts were washed several times with a cold mixture of H_2O/EtOH (50:50, v/v) and dried at 60 ºC for 12 h. The resulting

catalysts were denoted as Pd/H-ZSM-5, Pd/Na-ZSM-5, Pd/Cs-ZSM-5, Pd/H-Y, Pd/Na-Y and Pd/Cs-Y.

2.4. Catalysts characterisation

Catalysts supports based on zeolites Y and ZSM-5 were characterised by XRD, using a 2002 Seifert powder diffractometer to ensure that the ion exchange did not modify the zeolites structure. The scanning rate was 2ºC/min and Cu-Kα radiation was used.

The textural characterisation of the zeolitic supports was carried out by means of adsorption of N_2 at -196 ºC and CO_2 at 0 ºC (Autosorb 6, Quantachrome). Prior to the adsorption measurements, the supports were outgassed *in-situ* under vacuum at 250 ºC for 4 h in order to remove any adsorbed impurities. Apparent surface area values were calculated from nitrogen adsorption isotherms using the BET equation (S_{BET}). Total micropore volume ($V_{DR}(N_2)$) and narrow micropore volume ($V_{DR}(CO_2)$) were calculated applying the Dubinin–Radushkevich (DR) equation to the N_2 adsorption data at -196 ºC and the CO_2 adsorption data at 0 ºC, respectively.

Transmission electron microscopy (TEM) images were obtained by using a JEOL (JEM-2010) equipped with an EDS analyser (OXFORD, model INCA Energy TEM 100) operating at 200 kV with a space resolution of 0.24 nm. In order to prepare the samples for TEM analysis, a small amount of the catalyst was suspended in ethanol and sonicated in an ultrasonic bath for few minutes. After that, a drop of this suspension was deposited onto a 300 mesh Lacey copper grid and dried at room temperature. TEM images were also captured for the palladium colloid in order to compare the NP diameter and particle size distribution before and after the impregnation step.

The dispersion of the palladium nanoparticles on the catalysts (D), which is an estimation of the amount of metal exposed in the nanoparticles, was calculated from the following equation and assuming spherical shape of the particles (d; particle diameter) [24].

$$D(\%) \approx \frac{0.9}{d(nm)}$$

ICP-OES (Inductively Coupled Plasma-Optical Emission Spectroscopy) was the selected technique to determine the palladium loading. For this purpose, a Perkin Elmer

Optima 4300 system was used. The palladium extraction was carried out by oxidative treatment with aqua regia for 48 h. Then, the samples were filtered and diluted.

XPS (X-ray photoelectron spectroscopy) data were recorded using a VG-Microtech Multilab 3000 spectrometer equipped with a semispherical electron analyzer and a Mg Kα (hυ = 1253.6 eV) 300 W X-ray source. Before recording the spectra, the samples were maintained in the analysis chamber until a residual pressure of 5 x 10^{-9} mbar was reached. The spectra were collected at a pass energy of 50 eV. Binding energies were referenced to the C 1s line at 284.6 eV, which provide values with an accuracy of 0.2 eV. The Pd(0)/Pd(II) ratios were calculated from the integrated intensities of the spectra.

All the characterisation techniques were performed on the as-synthesised (non-reduced) catalysts.

2.5. Catalytic tests

All the catalysts were tested in the Preferential CO Oxidation reaction (PrOx-CO). The reactor used was a U-shaped reactor (16 mm inner diameter), where 150 mg of sample were placed. The samples were reduced with H_2, using a flow of 50 ml/min of 10 % H_2/He, in order to obtain reduced palladium nanoparticles. After that, the samples were cooled to room temperature and the reactant gas mixture (composed of 2 % CO, 2 % O_2, 30 % H_2, balance He) was passed through the catalysts. The oxygen excess, defined by the following equation, was λ = 2 (being λ = 1 for stoichiometric conditions).

$$\lambda = \frac{2\,[O_2]_0}{[CO]_0}$$

The gas composition is a hydrogen rich feed, in order to closely mimic the conditions used in the water gas shift reactor in the hydrogen purification process for fuel cell applications. The catalytic tests were performed using a heating rate of 2 ºC/min and a total gas flow rate of 100 ml/min that was set by means of mass flow controllers (MFCs, Bronkhorst). Catalytic activity was also expressed as TOF (in s^{-1}), defined as moles of CO consumed per moles of surface metal per second. The exhaust gases were analysed by gas chromatography (Agilent Technologies 6890N equipped with a CTRI column operating at 80 ºC and a TCD detector). Moreover the samples with the best catalytic behaviour were tested under a more complex gas mixture (composed of 2 % CO, 2 % O_2, 30 % H_2, 20 % CO_2, 5 % H_2O and balance He) and

carrying out long term stability experiments at 200 °C and with a total flow rate of 50 ml/min, in order to check the effect of CO_2 and H_2O in the catalytic performance in the PrOx-CO reaction. The measured inlet and outlet concentrations were used to calculate the CO conversion and selectivity, according to the following equations:

$$CO\ Conversion\ (\%) = \frac{[CO]_0 - [CO]}{[CO]_0} * 100$$

$$CO\ Selectivity\ (\%) = \frac{[CO]_0 - [CO]}{2([O_2]_0 - [O_2])} * 100$$

All experiments were performed by duplicate to ensure the reproducibility of the results.

3. Results

3.1 Colloid characterisation

A palladium colloid sample was prepared by the reduction by solvent method. This is a synthetic protocol that allows preparing metallic nanoparticles with a very small particle size and a narrow size distribution. Figure 1 shows a TEM image of the Pd nanoparticles colloid prepared for this work, and the histogram corresponding to the particle size distribution. As it can be observed from the image, the nanoparticles show a small average particle size (d=1.8±0.3nm), and a very narrow size distribution, as expected according to other authors reports [22], and observed by us in previous works [7] [25].
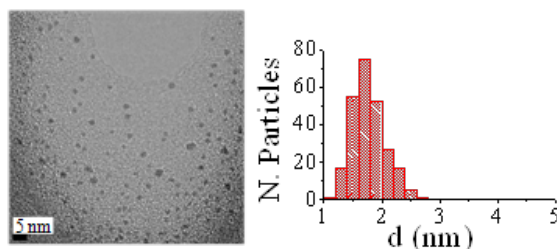
Figure1. TEM image of the as-prepared Pd nanoparticles colloid and the corresponding histogram.

As previously mentioned, nanoparticles prepared by the reduction by solvent method are highly stable against sintering and no agglomeration of the particles has been detected for periods of time over one year.

3.2 Support characterisation.

In order to observe the effect of ion-exchange in the crystallinity of the ZSM-5 and Y zeolites, XRD analyses were performed on the different supports. As it was expected, the ion exchange steps (and the heat treatment performed to convert the ammonium form of the ZSM-5 zeolite in the acid counterpart) did not modify the zeolites crystallinity, as it could be extracted from the comparison between the XRD patterns found in the literature (See Figure S1 in Supporting Information). Nevertheless when both zeolites were exchanged with cesium (supports denoted Cs-ZSM-5 and Cs-Y, respectively) a marked decrease in the number and intensity of the XRD peaks is observed compared to the parent commercial zeolites. It should be pointed out that when the ion exchange with cesium is carried out, the used salt contains trace amounts of Ba^{2+}, which has been reported to significantly alter the zeolitic structure [26]. As it was reported in the literature, the change in the relative intensities of the peaks when ion-exchange is performed could be due to the fact that the inclusion of a larger cation in the zeolite network can partially distort the structure because it must be accommodated into the zeolite structure [27]. Moreover, the XRD peaks intensity decrease has been also attributed to the strong absorption of X-ray by Cs [28].

Concerning the textural properties, Table 1 summarizes the BET surface area (S_{BET}), the total micropore (V_{DR} (N_2)) and the narrow micropore volume ($V_{DR}(CO_2)$) of the supports and Figure 2 includes the N_2 adsorption-desorption isotherms at -196 ºC.

Table 1. Porous texture characterisation results.

SAMPLE	S_{BET} (N_2) (m^2/g)	V_{DR} (N_2) (cm^3/g)	V_{DR} (CO_2) (cm^3/g)
H-ZSM-5	398	0.17	0.15

|			
Na-ZSM-5	373	0.17	0.14
Cs-ZSM-5	344	0.16	0.12
H-Y	724	0.35	0.41
Na-Y	721	0.35	0.31
Cs-Y	499	0.24	0.20

Comparing zeolites ZSM-5 and Y with the same cation exchanged, in all cases the surface area and pore volume of ZSM-5 samples are much lower than those of Y zeolite, as expected from the different structure [29]. However, the MFI-type zeolites display a small amount of mesoporosity (as evidenced from the hysteresis loop found for relative pressure values between 0.5-0.95) which is not present in its FAU-type counterpart. On the other hand, in the subsequent ion-exchange steps (from H-zeolites to Na-zeolites and from Na-zeolites to Cs-zeolites) a decrease of surface area is observed. These results can be explained by the difference of cation sizes, since the cation diameter of H^+ (0.012 Å) is much smaller than that of Na^+ (1.9 Å) and Cs^+ (3.3 Å) [30] and when these bigger cations occupy the sites inside the zeolite channel a decrease in surface area and pore volume is provoked [31]. The decrease in surface area and micropore volume in sample Cs-Y is much more important than in sample Cs-ZSM-5. It is important to take into account that in the ZSM-5 zeolite the cations are preferentially located in the intersection of the sinusoidal and straight channels at the edge of the four-member ring while, in the Y zeolite, the cation can be located in three different sites: on the hexagonal prism faces between the sodalite units, in the open hexagonal faces and on the wall of the supercage [32]. Thus, the presence of Cs^+ in some of these ion-exchange sites in Y zeolite, together with the higher ion-exchange capacity of this zeolite compared to ZSM-5, could lead to the partial blockage of the porosity [32].
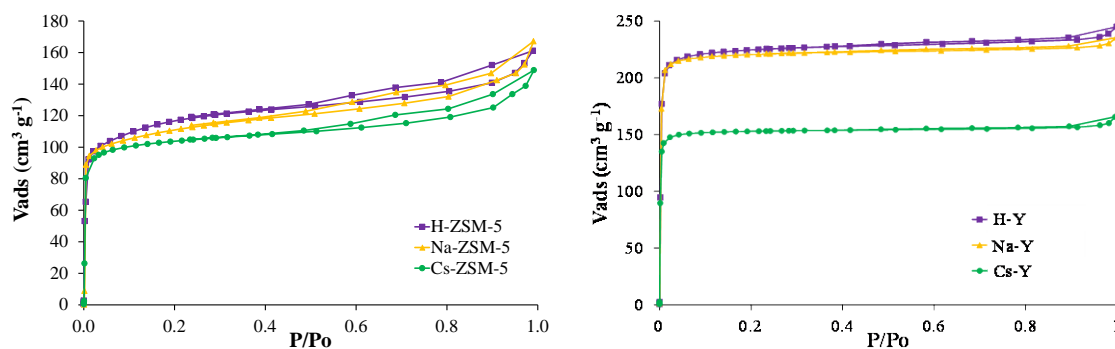
Figure 2. N_2 adsorption–desorption isotherms at -196 ºC corresponding to H-Y, Na-Y and Cs-Y catalysts supports.

3.3 Catalysts characterisation

Concerning the catalysts characterisation, Figure 3 includes the TEM micrographs of the fresh ion-exchanged ZSM-5 and Y catalysts and the pertinent histograms with the particle size distributions.
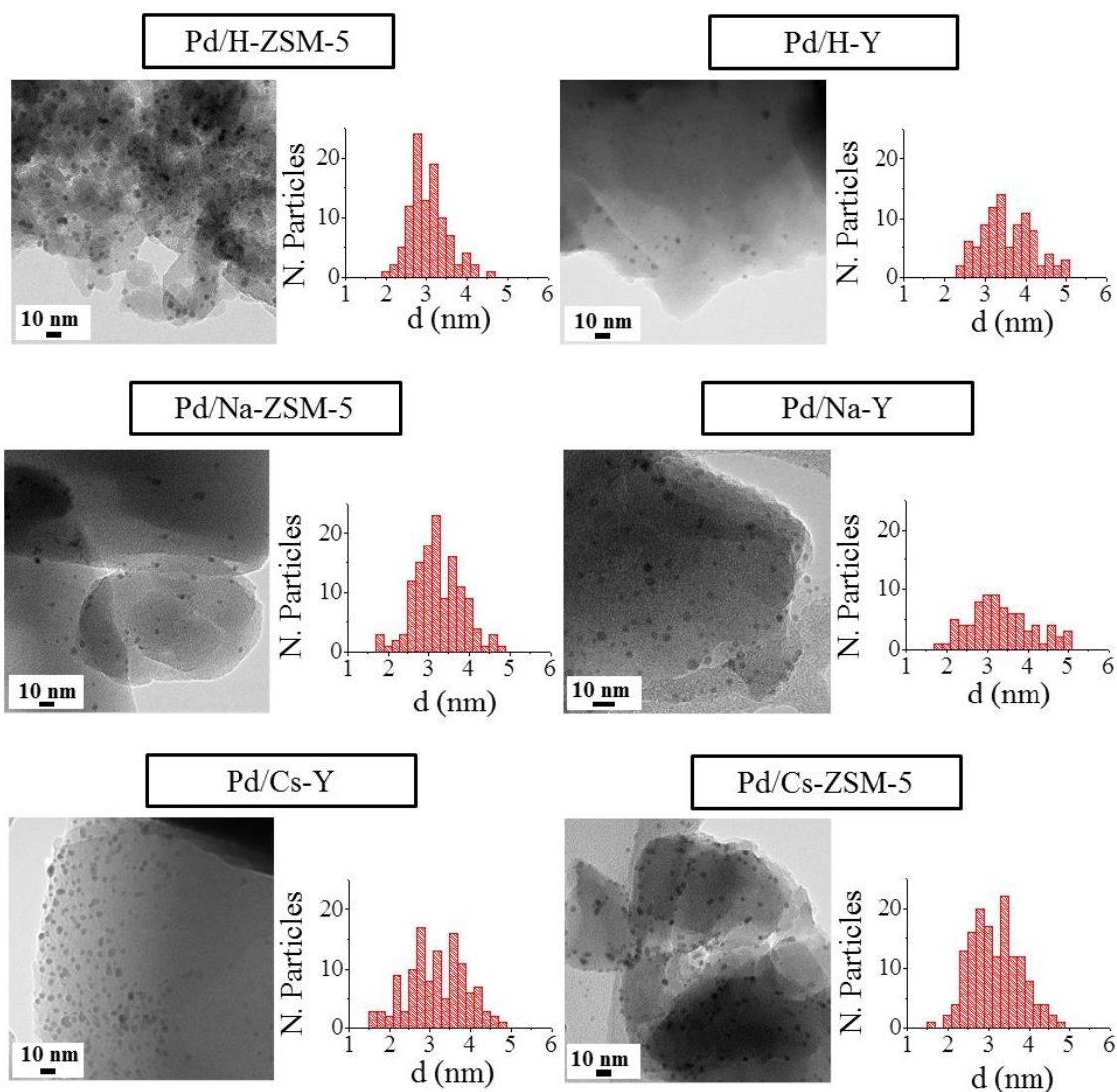
Figure 3. TEM images and Pd nanoparticles size distribution in the fresh ion-exchanged ZSM-5 and Y zeolites.

As it was previously reported by our research group for similar Pd/zeolite-based catalytic systems [25], Pd nanoparticles supported on zeolites show a very narrow size distribution and aggregates of palladium nanoparticles are not formed as a consequence of the impregnation or drying steps. However, a slight loss of their spherical shape when they are compared to the Pd nanoparticles in the metallic colloid can be appreciated, which might be favoured by the interaction between metal and support surface [7].

In addition, in order to assess the effect of the experimental conditions used in the catalytic tests in the Pd nanoparticles morphology, TEM analysis of used Pd/H-Y and Pd/Na-Y samples was also performed and the results are shown in Figure 4.
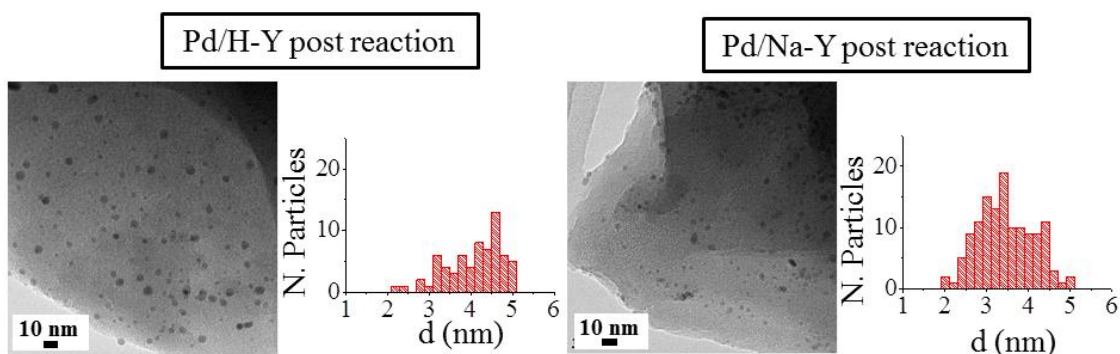
Figure 4. TEM images of samples Pd/H-Y and Pd/Na-Y after being used in the catalytic test and the pertinent histograms with the particle size distributions.

The recorded TEM images of used Pd/H-Y and Pd/Na-Y samples revealed that in both catalysts, the same palladium nanoparticles morphology as in the case of fresh samples were observed, but an important particle size increase for used Pd/H-Y sample was shown. Moreover, in order to check whether the nanoparticle size increase observed in sample Pd/H-Y after being tested was due to the reaction conditions used or to the previous catalyst pretreatment, TEM analysis of sample Pd/H-Y after being pretreated with 10 % H_2/He at 200 ºC was also carried out (Figure not shown here; see Table 2 for more details).

Table 2 summarizes the nanoparticles sizes for all the studied catalysts (fresh and used in the case of Pd/H-Y and Pd/Na-Y samples), the dispersion calculated from the TEM images and the metal loading determined by means of ICP.

Table 2. Particle size (d_{TEM}), dispersion (D_{TEM}) and metal loading of the catalysts.

SAMPLE	d_{TEM}(nm)	D_{TEM} (%)	Metal loading ICP (wt.%)
Pd/H-ZSM-5 (fresh)	3.1 ± 0.5	29.0	0.68
Pd/Na-ZSM-5 (fresh)	3.2 ± 0.6	28.1	0.45
Pd/Cs-ZSM-5 (fresh)	3.2 ± 0.6	28.1	0.42
Pd/H-Y (fresh)	3.8 ± 0.9	23.7	0.46
Pd/H-Y (pretreated)	4.2 ± 1.0	21.4	-
Pd/H-Y (post reaction)	4.9 ± 1.1	18.4	-
Pd/Na-Y (fresh)	3.5 ± 1.0	25.7	0.57
Pd/Na-Y (post reaction)	3.5 ± 0.7	25.7	-
Pd/Cs-Y (fresh)	3.3 ± 0.8	27.3	0.71

As it can be seen from the data included in Table 2, the nanoparticles size and dispersion are very similar in all the fresh catalysts. Comparing the nanoparticles size in the catalysts and in the metal colloid, an important particle size increase is produced when the palladium nanoparticles are supported onto the different zeolites (colloid, d=1.8±0.3nm). This size increase could be a consequence of the impregnation process, where some nanoparticles deformation can take place leading to the observation of apparent larger metal nanoparticles. Furthermore, considering the nanoparticles size observed in all the catalysts and the aforementioned zeolites opening channels diameters, it is expected that in all the catalysts the palladium nanoparticles are located on the zeolites external surface.

Regarding the post-reaction TEM analysis, some differences are observed for the used samples. In this sense, changes of nanoparticles size for sample Pd/Na-Y after being used in the catalytic test reaction were not observed, showing an average nanoparticle size of 3.5 nm for both, fresh and used samples. On the other hand, in the case of sample Pd/H-Y the palladium nanoparticle size is not constant for the sample in all the stages. Fresh Pd/H-Y sample showed a nanoparticle size of 3.8 nm, while a slight

increase was observed after the pretreatment with 10 % H_2/He at 200 ºC (average particle size 4.2 nm). Moreover, TEM characterisation of the sample after being used in the catalytic tests indicated that the palladium nanoparticles size increases even more (average particle size 4.9 nm) after being tested under the experimental conditions used (gas mixture composed of 2 % CO, 2 % O_2, 30 % H_2, and balance He and heated up to 200 ºC). The results indicate that the palladium nanoparticles stability, in terms of anchorage on the support, strongly depends on the cation present in the zeolite Y. In this regard, it seems that palladium nanoparticles are more stabilised on the Na-Y than on H-Y support, which may be related to the stronger Pd/PVP-system interaction with Na/Y than with H/Y, which seems to have a metal nanoparticles sintering inhibition ability. In this sense, the dependence of the Pd/PVP nanoparticles systems stability and particle size on the support characteristics for different metal oxide supports has been already reported [33].

Concerning the Pd loading, the ICP spectroscopy results indicated that it ranged from 0.42 to 0.71 wt.% even though all the catalysts were prepared to contain 1 wt.% of Pd.

In order to analyse the nature of the Pd contained in the different catalysts, XPS analyses of the fresh samples were performed. A typical XPS spectrum of a Pd-based catalyst shows two electronic transitions corresponding to the bands $Pd3d_{3/2}$ (at higher binding energies) and $Pd3d_{5/2}$ (at lower binding energies). Each of those transitions can be deconvoluted into two different peaks that are associated to electronically different Pd species, in agreement with previous results [7, 8]. The peak appearing at lower binding energies relates to Pd(0) and the peak at higher binding energies corresponds to Pd(II). In all the catalysts analysed in this study both Pd species (Pd(0) and Pd(II)) have been found by XPS analyses. Table 3 contains the results corresponding to the atomic percentage of the different Pd species present on the catalysts surface.

Table 3. XPS analysis of the as-prepared catalysts.

| SAMPLE	Pd (0) (atomic %)	Pd (II) (atomic %)
Pd/H-ZSM-5	76	24
Pd/Na-ZSM-5	74	26
Pd/Cs-ZSM-5	84	16
Pd/H-Y	80	20
Pd/Na-Y	91	9
Pd/Cs-Y	81	19

Previous studies performed in our research group pointed out that after the reduction pre-treatment carried out before testing the catalysts, the Pd(II) (or Pd with some positive charge, $\delta+$) contained in the samples is still present, so total metal reduction does not take place under the conditions used [7]. This is due to the presence of PVP surrounding the nanoparticles. The excess of PVP that is used as surfactant during the synthesis of nanoparticles is removed in the purification step. However, some of the PVP molecules linked to the metal surface remain, and therefore when the nanoparticles are deposited onto the supports, some surfactant molecules are also present. The interaction between the PVP polymer and Pt and Rh metal nanoparticles has been widely studied in the literature [34, 35]. This interaction consists in the PVP withdrawing electronic density from the metal surface through the CO groups contained in the monomers. We have previously demonstrated that this is also the case with Pd nanoparticles [7, 8]. This interaction leaves the metal surface with a deficiency of electronic density, and in an XPS spectrum these metal species appear as partially oxidized Pd (Pd(II)).

Moreover, the contribution of Pd (II) seems to depend on the catalyst support. In this sense, it could be said that in general, the Pd (II) contribution is slightly higher in the case of samples based on ZSM-5 zeolite than in the other catalysts.

3.4 Catalytic tests

Catalytic tests were performed for all the catalysts prepared for this work. In addition, control experiments with the bare zeolitic supports were carried out to confirm that the inactivity of the supports and, as expected, no catalytic activity was observed for any of them.

Figure 5 shows the catalytic performance (expressed as CO conversion and selectivity) of the palladium nanoparticles deposited on the differently ion-exchanged zeolites (ZSM-5 and Y, respectively).
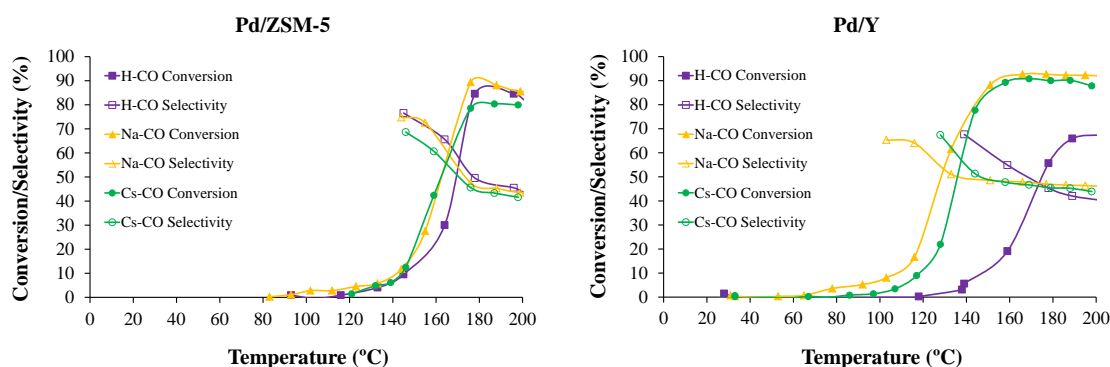
Figure 5. CO conversion (%, solid symbols) and selectivity (%, hollow symbols) of the different ion-exchanged ZSM-5 and Y catalysts.

The figure represents CO conversion and selectivity of the different ion-exchanged ZSM-5 and Y catalysts as a function of temperature. Both profiles are very important to determine the suitability of the catalysts for the PrOx-CO reaction. In this sense, the selectivity towards CO oxidation as a function of the temperature is an important parameter in the PrOx reaction, since the O_2 in the gas stream can be used not only for the CO oxidation to CO_2, but also for the concurrent H_2 oxidation, which leads to important drawbacks from both a technological and economical point of view [7].

It can be observed in Figure 6 that both, CO conversion and selectivity towards CO oxidation, strongly depend on the temperature. In this sense, the CO conversion reaches a maximum at a certain temperature (which is different for all the samples) and then decreases slowly. The selectivity also decreases at high temperatures for all the catalysts, what suggests that the H_2 oxidation becomes more favoured at high temperatures due to the higher activation energy of the H_2 oxidation with respect to the CO oxidation reaction [7, 20, 36].

In order to assess the catalytic performance from a more comparative point of view, TOF (s^{-1}) values calculated at 125 ºC are included in the Table 4. In addition, maximum CO conversion (%), maximum CO selectivity (%) and selectivity (%) at 25 % of CO conversion are also added in the same Table.

Table 4. Catalytic results in PrOx reaction and TOF (s^{-1}) calculated at 125 ºC.

SAMPLE	Maximum CO conversion (%)	Maximum CO selectivity (%)	Selectivity (%) at 25 % of CO conversion	TOF (s^{-1}) 125 ºC
Pd/H-ZSM-5	85 (178 ºC)	77 (145 ºC)	67 (161 ºC)	0.01
Pd/Na-ZSM-5	89 (176 ºC)	75 (144 ºC)	73 (154 ºC)	0.04
Pd/Cs-ZSM-5	80 (187 ºC)	69 (146 ºC)	65 (152 ºC)	0.03
Pd/H-Y	67 (200 ºC)	67 (139 ºC)	53 (163 ºC)	0.02
Pd/Na-Y	93 (166 ºC)	65 (103 ºC)	61 (120 ºC)	0.16
Pd/Cs-Y	91 (169 ºC)	67 (117 ºC)	66 (129 ºC)	0.10

The maximum CO conversions obtained are very high for all the catalysts studied, except for sample Pd/H-Y, reaching values very close to 90 % and even higher for samples with Y zeolite. However, the temperature at which this maximum conversion is reached is different for all the catalysts. In this sense, if samples with the same zeolite structure and different ion-exchange cations are considered, it seems that zeolites ion-exchanged with sodium reach higher CO conversion and that these maximum conversion values are achieved at lower temperatures than in the other samples.

Regarding selectivity, relatively high values of selectivity are also reached for all the catalysts, being higher for catalysts prepared with ZSM-5 zeolite. To better evaluate these values it is important to highlight that, under the experimental conditions used, an adequate catalyst for this reaction should have selectivity values towards CO oxidation over 50 %, which means that CO oxidation is preferential over H_2 oxidation and that, theoretically, all CO could be removed from the H_2 flow [37]. In the studied samples, maximum selectivity values towards CO oxidation between 65 and 77 % were achieved at low CO conversion (low temperatures) and selectivity values very close to 50 %

remain at higher temperatures (see Figure 5). Thus, bearing these results in mind and comparing with those reported elsewhere, where different catalytic systems were studied [7, 10, 38], it could be said that the prepared catalysts are very promising materials for their use in the PrOx-CO reaction, especially in the case of samples ion-exchanged with sodium.

Taking into account the results enclosed in Table 4, it seems that the addition of cations with lower charge density in the zeolite structure plays a positive role in the catalytic behaviour of the sample. This improvement when cations with lower charge density are added has been observed by other authors for samples based on zeolites [39] and other systems [40-42]. As it can be seen, this improvement mainly reflects on the selectivity at 25 % of CO conversion and TOF parameters. As it can be extracted from Table 4, the selectivity values achieved for 25 % of CO conversion are between 53 and 73 % for the six studied samples and, in general the achieved values are higher in samples with ZSM-5 zeolite. In samples based on ZSM-5 zeolite, this value of CO conversion is achieved at very similar temperatures for the three studied samples, but the selectivity is higher in sample Pd/Na-ZSM-5. Regarding the samples based on Y zeolite, the 25 % of CO conversion is achieved at temperatures much lower in the case of the samples ion-exchanged with Na^+ and Cs^+ cations (120 and 129 ºC, for samples Pd/Na-Y and Pd/Cs-Y, respectively) than for the protonated counterpart (163 ºC). In the case of sample Pd/H-Y an important shift towards higher temperatures is observed for CO conversion and selectivity curves. This poor behaviour of sample Pd/H-Y, under the experimental conditions used, may be related to the palladium nanoparticles sintering observed for this sample (see Table 2) when it is pretreated in 10 % H_2/He at 200 ºC and under the subsequent catalytic test experimental conditions (gas mixture composed of 2 % CO, 2 % O_2, 30 % H_2, and balance He and heated up to 200 ºC), probably as a consequence of the weaker interaction between the palladium nanoparticles and the H-Y support compared to the support Na-Y. This fact indicates that the catalytic performance of the studied samples in the preferential CO oxidation reaction strongly depends on the average palladium nanoparticle size, as it was previously reported by our group [7].

Concerning the TOF parameter, it can be observed that when the catalytic activity is normalised taking into account the metallic loading of the samples and the size of the particles, all the ZSM-5 catalysts show a much poorer behaviour in terms of activity than the Y catalysts.

Bearing in mind the support pore size and the Pd nanoparticles size, it is clear that, as it was previously said, Pd nanoparticles are located on the outer zeolite surface. Thus, the location of the nanoparticles pointed out that inner surface area of the zeolites does not play a significant role in the oxidation of CO. However, the outstanding catalytic performance of samples based on Y zeolite, (mainly in terms of TOF) could be related to the larger surface area of this zeolite. According to the porous texture characterisation results (see Table 1), samples based on Y zeolite may adsorb larger amounts of CO molecules in their porous structure. This larger presence of CO accumulated within the porous structure in samples with Y zeolites could tentatively explain the improved catalytic activity of these samples.

Once the results obtained in this work have been presented and discussed, a comparison with results reported in the literature should be carried out in order to highlight the strength of the studied Pd/zeolite-based catalytic systems in the PrOx-CO reaction. In this regard, the use of zeolitic materials as support for catalysts used in the PrOx-CO reaction is not very widely reported, being Al_2O_3 combined with different noble metal [7, 10, 43], and CuO/CeO_2 [44-46] the most common catalytic systems used for this application. Concerning the zeolitic system, the metallic active phase is normally incorporated by ion exchange procedure, thus the metal might be located inside the zeolite porosity, leading to a lower catalytic performance, as it was claimed by Luengnaruemitchai et al. [20]. These authors prepared A-type zeolite-supported Pt catalysts by the impregnation method, and the metal was placed outside the pore of LTA as in the case of the palladium nanoparticles used in the present study. In that study, the catalytic activity was evaluated using a gas mixture composed by 1 % CO, 1 % O_2, 40 % H_2 and He (balance) at a total flow rate of 50 ml/min. Under these experimental conditions, almost 100 % of CO conversion and ~ 50 % of selectivity were achieved at 200 ºC approximately. Moreover, Rosso el al. [19] prepared Pt/3A catalysts by different experimental procedures, cation exchange, wet impregnation and incipient wetness impregnation. The obtained results also indicated that the metal location and the catalytic performance depend on the experimental method used to load the metallic phase. The result reported in that work claimed that the location of Pt particles outside the zeolite pores, resulting by the wet impregnation and incipient wetness impregnation methods, has a positive effect in the preferential CO oxidation. Similar results were also obtained by Rivallan et al. [47] for Pt nanoparticles incorporated

on ZSM-5. Kotobuki and coworkers [48] studied a catalytic system based on Pt-Fe alloy nanoparticles supported on mordenite, with a very high metal loading in comparison with the present work (4 and 0.5 wt. % for Pt and Fe, respectively) and they confirmed that the CO conversion depends on the oxygen excess (λ). When $\lambda = 2$, as in the present study, they achieved about 100 % of CO conversion and ~ 50 % of CO selectivity at about 100 ºC, but these values decreased drastically to ~ 67 % of CO conversion and ~ 25 % of CO selectivity at 200 ºC.

The suitable catalytic performance of the samples studied in this work is also evidenced by the comparison with other catalytic systems studied in the literature, where different supports apart from zeolites are studied. In this sense, the comparison with the results previously obtained in our group using palladium nanoparticles supported on alumina catalysts [7], where a 55 % of selectivity was achieved for a 25 % of CO conversion, reveals that the present catalytic systems are very promising materials for their use in the PrOx-CO reaction.

After presenting the screening of the catalytic behaviour in the PrOx-CO reaction of the samples studied in this work and comparing with those previously reported in the literature, it can be said that the Pd/zeolite-based samples are very promising catalysts in the Preferential CO Oxidation reaction, being sample Pd/Na-Y the most interesting catalyst. In this point, once the Pd/Na-Y sample was identified as the most effective catalyst, stability test of this sample was also performed and included in Figure 6.
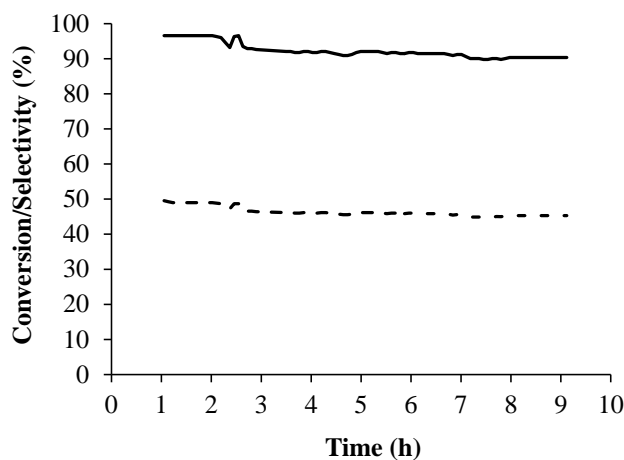
Figure 6. Stability test of sample Pd/Na-Y carried out at 200 ºC and with a gas mixture composed of 2 % CO, 2 % O_2, 30 % H_2, 20 % CO_2, 5 % H_2O and balance He. CO conversion (%) is plotted as a continuous line and selectivity (%) as a dotted line.

The stability test results obtained for sample Pd/Na-Y indicated that the decrease of both CO conversion and selectivity is not very pronounced (CO conversion from 96 % to 90 %; CO selectivity from 50 % to 45 %) when the sample is subjected to the working conditions used. Thus, no deactivation was observed for sample Pd/Na-Y during the 9 h of experiment, even when CO_2 and H_2O are added in the gas mixture. The high stability observed for sample Pd/Na-Y suggests that there is no sintering or coke formation on the catalyst during the reaction. Therefore, it can be said that this is a promising material as catalyst in the PrOx-CO reaction, since high CO conversion and selectivity values are achieved, which remain over long-term stability test.

4. Conclusions

Samples based on palladium nanoparticles supported on ion-exchanged ZSM-5 and Y zeolites have been prepared and tested in the PrOx-CO reaction. The obtained results seem to indicate that the catalytic performance of this type of materials depends on the zeolite structure, the composition and on the cation present in the zeolite.

All the studied samples showed a very promising catalytic performance, with the exception of sample Pd/H-Y, which displayed a poor catalytic behaviour due to the palladium nanoparticles sintering, caused probably by the weaker interaction with the zeolitic support.

The screening of the Pd/zeolite-based catalysts in the PrOx-CO reaction in H_2-rich streams, showed the suitability of zeolites as supports for the PVP-capped Pd nanoparticles, as very interesting catalytic performances were observed for all the studied catalysts. In particular, the outstanding catalytic behaviour displayed by the sample Pd/Na-Y in the long-term stability tests, indicated that this is a promising catalyst in the PrOx-CO reaction, as high CO conversion and CO selectivity values were achieved during long period of time.

21

References

[1]   Arango-Díaz, A.; Moretti, E.; Talon, A.; Storaro, L.; Lenarda, M.; Núñez, P.; Marrero-Jerez, J.; Jiménez-Jiménez, J.; Jiménez-López, A.; Rodríguez-Castellón, E., *Applied Catalysis A: General*, (2014) **477**, 54.
[2]   Rosso, I.; Galletti, C.; Saracco, G.; Garrone, E.; Specchia, V., *Applied Catalysis B: Environmental*, (2004) **48**, 195.
[3]   Liu, K.; Wang, A.; Zhang, T., *ACS Catalysis*, (2012) **2**, 1165.
[4]   Park, E. D.; Lee, D.; Lee, H. C., *Catalysis Today*, (2009) **139**, 280.
[5]   Mariño, F.; Descorme, C.; Duprez, D., *Applied Catalysis B: Environmental*, (2004) **54**, 59.
[6]   Pozdnyakova, O.; Teschner, D.; Wootsch, A.; Kröhnert, J.; Steinhauer, B.; Sauer, H.; Toth, L.; Jentoft, F. C.; Knop-Gericke, A.; Paál, Z.; Schlögl, R., *Journal of Catalysis*, (2006) **237**, 17.
[7]   Miguel-García, I.; Berenguer-Murcia, Á.; Cazorla-Amorós, D., *Applied Catalysis B: Environmental*, (2010) **98**, 161.
[8]   Miguel-García, I.; Berenguer-Murcia, Á.; García, T.; Cazorla-Amorós, D., *Catalysis Today*, (2012) **187**, 2.

[9]   Kipnis, M.; Volnina, E., *Applied Catalysis B: Environmental*, (2010) **98**, 193.
[10]   Manasilp, A.; Gulari, E., *Applied Catalysis B: Environmental*, (2002) **37**, 17.
[11]   Kim, Y. H.; Park, E. D., *Applied Catalysis B: Environmental*, (2010) **96**, 41.
[12]   Igarashi, H.; Uchida, H.; Suzuki, M.; Sasaki, Y.; Watanabe, M., *Applied Catalysis A: General*, (1997) **159**, 159.
[13]   Watanabe, M.; Uchida, H.; Ohkubo, K.; Igarashi, H., *Applied Catalysis B: Environmental*, (2003) **46**, 595.
[14]   López-Fonseca, R.; Gutiérrez-Ortiz, J. I.; Gutiérrez-Ortiz, M. A.; González-Velasco, J. R., *Catalysis Today*, (2005) **107–108**, 200.
[15]   Ribeiro, F.; Silva, J. M.; Silva, E.; Vaz, M. F.; Oliveira, F. A. C., *Catalysis Today*, (2011) **176**, 93.
[16]   Saepurahman; Visur, M.; Olsbye, U.; Bjørgen, M.; Svelle, S., *Top Catal*, (2011) **54**, 1293.
[17]   Čejka, J.; Centi, G.; Perez-Pariente, J.; Roth, W. J., *Catalysis Today*, (2012) **179**, 2.
[18]   Xu, J.; Xu, X.-C.; Ouyang, L.; Yang, X.-J.; Mao, W.; Su, J.; Han, Y.-F., *Journal of Catalysis*, (2012) **287**, 114.
[19]   Rosso, I.; Galletti, C.; Fiorot, S.; Saracco, G.; Garrone, E.; Specchia, V., *J Porous Mater*, (2007) **14**, 245.
[20]   Luengnaruemitchai, A.; Nimsuk, M.; Naknam, P.; Wongkasemjit, S.; Osuwan, S., *International Journal of Hydrogen Energy*, (2008) **33**, 206.
[21]   Naknam, P.; Luengnaruemitchai, A.; Wongkasemjit, S.; Osuwan, S., *Journal of Power Sources*, (2007) **165**, 353.
[22]   Lu, P.; Teranishi, T.; Asakura, K.; Miyake, M.; Toshima, N., *The Journal of Physical Chemistry B*, (1999) **103**, 9673.
[23]   Domínguez-Domínguez, S.; Berenguer-Murcia, Á.; Cazorla-Amorós, D.; Linares-Solano, Á., *Journal of Catalysis*, (2006) **243**, 74.
[24]   M. Boudart, Kinetics of Heterogeneous Catalytic Reactions, Princeton University Press, Princeton, NJ, 1984.
[25]   Navlani-Garcia, M.; Martis, M.; Lozano-Castello, D.; Cazorla-Amoros, D.; Mori, K.; Yamashita, H., *Catalysis Science & Technology*, (2015),
[26]   Varela-Gandía, F. J.; Berenguer-Murcia, A.; Lozano-Castelló, D.; Cazorla-Amorós, D., *Journal of Membrane Science*, (2010) **351**, 123.
[27]   Khaleghian-Moghadam, R.; Seyedeyn-Azad, F., *Microporous and Mesoporous Materials*, (2009) **120**, 285.
[28]   Bisio, C.; Martra, G.; Coluccia, S.; Massiani, P., *The Journal of Physical Chemistry C*, (2008) **112**, 10520.
[29]   Kim, Y. T.; Jung, K.-D.; Park, E. D., *Applied Catalysis A: General*, (2011) **393**, 275.
[30]   Xu, B.; Kevan, L., *The Journal of Physical Chemistry*, (1992) **96**, 2642.
[31]   Serra, R. M.; Miró, E. E.; Bolcatto, P.; Boix, A. V., *Microporous and Mesoporous Materials*, (2012) **147**, 17.
[32]   Xu, J.; Mojet, B. L.; Lefferts, L., *Microporous and Mesoporous Materials*, (2006) **91**, 187.
[33]   Siyo, B.; Schneider, M.; Radnik, J.; Pohl, M.-M.; Langer, P.; Steinfeldt, N., *Applied Catalysis A: General*, (2014) **478**, 107.
[34]   Borodko, Y.; Habas, S. E.; Koebel, M.; Yang, P.; Frei, H.; Somorjai, G. A., *The Journal of Physical Chemistry B*, (2006) **110**, 23052.
[35]   Borodko, Y.; Humphrey, S. M.; Tilley, T. D.; Frei, H.; Somorjai, G. A., *The Journal of Physical Chemistry C*, (2007) **111**, 6288.

[36]   Laguna, O. H.; Ngassa, E. M.; Oraá, S.; Álvarez, A.; Domínguez, M. I.; Romero-Sarria, F.; Arzamendi, G.; Gandía, L. M.; Centeno, M. A.; Odriozola, J. A., *Catalysis Today*, (2012) **180**, 105.

[37]   Kahlich, M. J.; Gasteiger, H. A.; Behm, R. J., *Journal of Catalysis*, (1997) **171**, 93.

[38]   Iwasa, N.; Arai, S.; Arai, M., *Applied Catalysis B: Environmental*, (2008) **79**, 132.

[39]   Lahr, D. G.; Li, J.; Davis, R. J., *Journal of the American Chemical Society*, (2007) **129**, 3420.

[40]   Kuriyama, M.; Tanaka, H.; Ito, S.-i.; Kubota, T.; Miyao, T.; Naito, S.; Tomishige, K.; Kunimori, K., *Journal of Catalysis*, (2007) **252**, 39.

[41]   Minemura, Y.; Kuriyama, M.; Ito, S.-i.; Tomishige, K.; Kunimori, K., *Catalysis Communications*, (2006) **7**, 623.

[42]   Derrouiche, S.; Gravejat, P.; Bassou, B.; Bianchi, D., *Applied Surface Science*, (2007) **253**, 5894.

[43]   Yin, J.; Wang, J.; Zhang, T.; Wang, X., *Catal Lett*, (2008) **125**, 76.

[44]   Monte, M.; Gamarra, D.; López Cámara, A.; Rasmussen, S. B.; Gyorffy, N.; Schay, Z.; Martínez-Arias, A.; Conesa, J. C., *Catalysis Today*, (2014) **229**, 104.

[45]   Zeng, S.; Wang, Y.; Ding, S.; Sattler, J. J. H. B.; Borodina, E.; Zhang, L.; Weckhuysen, B. M.; Su, H., *Journal of Power Sources*, (2014) **256**, 301.

[46]   Gong, L.; Huang, Z.; Luo, L.; Zhang, N., *Reac Kinet Mech Cat*, (2014) **111**, 489.

[47]   Rivallan, M.; Thomas, S.; Lepage, M.; Takagi, N.; Hirata, H.; Thibault-Starzyk, F., *ChemCatChem*, (2010) **2**, 1599.

[48]   Kotobuki, M.; Watanabe, A.; Uchida, H.; Yamashita, H.; Watanabe, M., *Applied Catalysis A: General*, (2006) **307**, 275.